

## On the Differences in Storm Rainfall from Hurricanes Isidore and Lili. Part II: Water Budget

HAIYAN JIANG AND JEFFREY B. HALVERSON

*Joint Center for Earth Systems Technology, University of Maryland, Baltimore County, Baltimore, and Mesoscale Atmospheric Processes Branch, NASA Goddard Space Flight Center, Greenbelt, Maryland*

JOANNE SIMPSON

*Laboratory for Atmospheres, NASA Goddard Space Flight Center, Greenbelt, Maryland*

EDWARD J. ZIPSER

*Department of Meteorology, University of Utah, Salt Lake City, Utah*

(Manuscript received 8 December 2005, in final form 16 May 2007)

### ABSTRACT

Part I of this two-part paper examined the satellite-derived rainfall accumulation and rain potential history of Hurricanes Isidore and Lili (2002). This paper (Part II) uses analyses from the Navy Operational Global Atmospheric Prediction System (NOGAPS) to examine the water budget and environmental parameters and their relationship to the precipitation for these two storms. Factors other than storm size are found to account for large volumetric differences in storm total rainfall between Lili and Isidore. It is found that the horizontal moisture convergence was crucial to the initiation and maintenance of Isidore's intense rainfall before and during its landfall. When the storm was over the ocean, the ocean moisture flux (evaporation) was the second dominant term among the moisture sources that contribute to precipitation. During Isidore's life history, the strong horizontal moisture flux convergence corresponded to the large storm total precipitable water. The large difference in budget-derived stored cloud ice and liquid water between Isidore and Lili is corroborated from Tropical Rainfall Measuring Mission (TRMM) measurements. During Isidore's landfall, the decrease in environmental water vapor contributed to rainfall in a very small amount. These results indicate the importance of the environmental precipitable water and moisture convergence and ocean surface moisture flux in generating Isidore's large rainfall volume and inland flooding as compared with Lili's water budget history. Both the moisture convergence and ocean flux were small for Lili.

### 1. Introduction

Understanding, examining, and predicting the variation of tropical cyclone precipitation requires some knowledge of the crucial environmental factors. These factors may help us understand the important mechanisms that discriminate among degrees of storm "wetness." The main environmental forcing mechanisms that exert a large influence on the variation of tropical cyclone precipitation are sea surface moisture flux (a

function of air and sea surface temperatures and surface winds), vertical wind shear, upper-tropospheric eddy-relative angular momentum flux convergence (ERFC), and tropospheric water vapor flux (Frank 1977). Many studies have shown that the sea surface temperatures (SSTs) warmer than 26°C and vertical wind shear of less than 10 m s<sup>-1</sup> are necessary conditions for initiating and maintaining inner-core convective bursts and outer-core convective rings (Emanuel 1986; Merrill 1988; Mundell 1991; Rodgers et al. 1994, 2000; Rodgers and Pierce 1995; Frank and Ritchie 2001). From observational studies of several hurricanes and tropical cyclones, Rodgers et al. (1994, 1998, 2000) and Rodgers and Pierce (1995) suggest that in regions of warm SSTs and weak vertical wind shear, the en-

---

*Corresponding author address:* Dr. Haiyan Jiang, Dept. of Meteorology, University of Utah, Rm. 819 WBB, 135 S 1460 E, Salt Lake City, UT 84112.  
E-mail: h.jiang@utah.edu

hancement of precipitation in tropical cyclone inner-core convective rainbands coincides with the inward convergence of ERFC, while the initialization of outer-core convective rainbands coincides with the horizontal moisture convergence. But recently it is found that weak shear is not necessary to initiate convective bursts (Heymsfield et al. 2005; Molinari et al. 2004).

The physical mechanism by which the upper-tropospheric forcing alters the tropical cyclone precipitation is believed to be related to the gradient wind adjustment process associated with the thermally direct circulation at the entrance region of tropical cyclones' outflow channels (Challa and Pfeffer 1980; Merrill 1988; Rodgers et al. 1991; DeMaria et al. 1993). The physical process that allows the lower-tropospheric forcing to alter the tropical cyclone rainfall is associated with surface evaporation (Frank 1977) and strong synoptic-scale water vapor convergence (Charney and Eliassen 1964; Molinari and Skubis 1985).

A moisture budget study is necessary to provide additional insight into the storm precipitation development and storm wetness parameter. Early water vapor budget studies for storms over land neglected the contribution from evaporation and suggested that the computed moisture convergence can be used for quantitative precipitation forecasting (Spar 1953; Bradbury 1957; Carr and Bosart 1978). However, for tropical cyclones over ocean, the ocean moisture flux is not negligible. Kurihara (1975) computed volumetric vapor budgets of a simulated axisymmetric hurricane. Although the dominant terms were the total advection (horizontal and vertical moisture transport) and the condensation, evaporation from the ocean surface was 20% and 25% of the condensation and total advection, respectively, for a 500-km-radius domain. If the domain of integration is reduced to the inner region, the relative magnitude of evaporation was very small compared with the condensation and total advection. This is consistent with the moisture budget estimation of Malkus and Riehl (1960) and Braun (2006). Their results showed that the ocean moisture flux is less than 10% of the net horizontal moisture convergence into the inner area. However, both Kurihara (1975) and Malkus and Riehl (1960) emphasized that a seemingly negligible amount of evaporation in the inner area can play a crucial role in the energetics of a tropical cyclone. It is reasonable to expect that the relative contribution of the ocean moisture flux will be larger if the domain of integration is expanded for larger-sized storms. Many other vapor budget studies of hurricanes also suggested that a substantial percentage (around 40%–50%) of the total condensation (precipitation plus cloud storage) was from the ocean moisture flux (Hawkins and Rub-

sam 1968; Hawkins and Imbembo 1976; Gamache et al. 1993).

However, almost all of the previous studies focused on one stage of a hurricane. Detailed moisture budget studies for the whole lifetimes of tropical cyclones are not well documented. In this study, the water budget histories of Hurricanes Isidore and Lili are assessed by using the Navy Operational Global Atmospheric Prediction System (NOGAPS) analysis and the satellite-derived National Aeronautics and Space Administration (NASA) Goddard real-time Multisatellite Precipitation Analysis (MPA-RT; Huffman et al. 2003, 2007) rainfall data. Our goal is to determine the crucial environmental factors that initiated and maintained the large differences of rainfall before and during the landfalls of Isidore and Lili. Environmental parameters derived from NOGAPS analyses such as total precipitable water (TPW), SST, vertical wind shear, sea surface – air moisture difference ( $\Delta q$ ), wind speed at 10 m above the surface (10-m wind speed), upper-tropospheric divergence, and near-surface  $\theta_e$  are examined to see how they are related to the differences in storm wetness and intensity for Isidore and Lili.

Jiang et al. (2008, hereafter Part I) describe the synoptic overview and MPA-RT-derived rainfall history and rain potential difference of Isidore and Lili. In this paper, section 3 presents the Tropical Rainfall Measuring Mission (TRMM)-based ice water path (IWP) and liquid water path (LWP) estimates, which could indirectly evaluate the cloud storage term estimation in the water budget calculations. The water budget terms based on the storm volumetric integral and radial distribution will be diagnosed for these two storms in section 4. The water budget result quantifies the significant contributions from moisture convergence and sea surface evaporation to the tropical cyclone rainfall. Section 5 investigates other environmental factors that influence Isidore and Lili's precipitation and intensification. Section 6 contains a brief summary of the results and conclusions.

## 2. Data and methodology

### a. Data description

#### 1) TRMM-BASED IWP AND LWP ESTIMATES

Launched in November 1997, the TRMM satellite has provided critical information regarding the 4D distributions of precipitation and latent heating in the tropics (Simpson et al. 1988, 1996; Kummerow et al. 1996, 2000). This study uses data from the two chief sensors on board TRMM: the Precipitation Radar (PR) and the TRMM Microwave Imager (TMI). The PR is a

3D precipitation radar with a frequency of 13.8 GHz. The PR provides reflectivities from the surface to 20 km above the earth ellipsoid. The TMI takes observations in nine channels at five frequencies: 10.7, 19.35, 21.3, 37.0, and 85.5 GHz. All frequencies are measured independently in the horizontal and vertical polarization planes, except the 21.3-GHz channel, which measures the radiance in the vertical polarization plane.

Jiang and Zipser (2006) developed a combined radar–radiometer algorithm to estimate the precipitation ice water content (IWC) and liquid water content (LWC) profiles in tropical cyclones and convection for aircraft-based observations. In the algorithm, the intercept parameter,  $N_0$ , in the exponential particle size distribution for rain, snow, and graupel is adjusted iteratively to minimize the difference between observed brightness temperatures ( $T_b$ 's) and simulated ones by using a simulated annealing optimization method. This algorithm was applied to the fourth Convection and Moisture Experiment (CAMEX-4) aircraft-based hurricane and tropical convection dataset and validated by in situ microphysical measurements. Jiang (2004) adapted this algorithm to TMI and PR observations. For each radar reflectivity profile observation, the TRMM PR qualitative algorithm (TRMM 2A23; Awaka et al. 1998) is used to determine the height and depth of the melting layer for each rain type. As long as the melting-layer information is obtained, LWC and IWC could be separated from the retrieved hydrometeor profile. Inside the melting layer, a linear interpolation is applied to calculate LWC and IWC. The ice (liquid) water path is obtained from the vertical integral of IWC (LWC). The IWP is water equivalent, which means that ice is melted into water to get the total IWP. In this study, this combined algorithm is used to estimate IWP and LWP for TRMM overpasses for Isidore on 22 September 2002 and for Lili on 2 October 2002. These estimates can be used indirectly to evaluate the stored liquid and ice water term in the water budget equation.

This algorithm can only retrieve the *precipitation* IWC/IWP and LWC/LWP because the TRMM PR and TMI mainly detect precipitation-size particles and cannot see small cloud size water particles. However, a statistical study based on the TMI rainfall algorithm (2A12; Kummerow et al. 1996) output for the 1-yr tropical cyclone database (Jiang 2004) shows that the cloud water content is between 5% and 20% of the rainwater content. The TRMM 2A12 algorithm is based on the 3D cloud model output. The estimates based on fragmentary cloud water data from the National Hurricane Research Project also show that the total water path held in the form of small cloud drops is

less by an order of magnitude than the total water path held in the form of precipitation size particles (B. Ackerman 2005, personal communication).

## 2) SSM/I-DERIVED TOTAL PRECIPITABLE WATER (TPW)

The Special Sensor Microwave Imagers (SSM/Is) on board the *F-13*, *F-14*, and *F-15* Defense Meteorological Satellite Program (DMSP) that were launched in May 1995, May 1997, and December 1999, respectively, measure scattered and emitted microwave radiation at frequencies of 19.35, 22.35, 37.0, and 85.5 GHz. All channels except the 22.35-GHz channel are dual polarized. The approximate time that the ascending branches of the DMSP *F-13*, *F-14*, and *F-15* orbits pass over the central Gulf of Mexico (i.e., 25°N, 90°W) where Isidore and Lili occurred are, respectively, 1200, 1400, and 1600 UTC. The approximate times of the descending branches of the DMSP orbits over Isidore and Lili are 12 h later. Further information about the SSM/I sensor and measurements may be found in Hollinger (1991). The SSM/I-estimated TPW over ocean regions is derived from version 5 of the Wentz SSM/I algorithm (Wentz 1997). The algorithm is based on a radiative transfer model for the brightness temperature of ocean and intervening atmosphere. The SSM/I algorithm cannot retrieve TPW over land or in raining areas.

### b. Water budget analysis method and environmental diagnostics

The environmental diagnostic and water budget parameters used for this study are obtained from the NOGAPS analyses (Rosmond 1992; Goerss and Phoebus 1992). The NOGAPS model is chosen for its high spatial resolution ( $1^\circ \times 1^\circ$  latitude–longitude grid) and its ability to accurately analyze tropical cyclones. The tropical cyclone observations are automatically generated and entered in the NOGAPS database for storms in the North and South Pacific, the Atlantic, and the Indian Oceans for all analyses of the real-time and post-time runs. The SSM/I-derived TPWs are assimilated into NOGAPS for global oceans. Both lower- and upper-level winds derived from geostationary satellite observations are assimilated into NOGAPS too. Currently, the SST analyses used in NOGAPS and in other large-scale models are very good (J. Goerss 2007, personal communication). Therefore, combining with the TRMM-based satellite rainfall estimates, the water budget should be reasonably calculated because NOGAPS assimilates synthetic tropical cyclone observations (Goerss and Jeffries 1994). Those environmental parameters as mentioned in section 1 and water bud-

get parameters are produced every 12 h (0000 and 1200 UTC) during each tropical cyclone day from the NOGAPS analyses.

### 1) DESCRIPTION OF WATER BUDGET

The atmospheric water budget is evaluated using a Lagrangian approach whereby the evolution of the water budget terms and their distribution of storms from genesis through maturity could be monitored. At each time step, the outline of the evaluation domain is at 1111-km radius from the storm circulation center, which is based on the best-track data from the National Hurricane Center.

An expression for the water vapor budget for the air volume follows from Rabin et al. (1993) and Halverson et al. (1996):

$$\frac{\partial(\text{TPW})}{\partial t} = F + Z + E - P - C, \quad (1)$$

where TPW is the total precipitable water (mm, equivalent to  $\text{kg m}^{-2}$ );  $F$  is the horizontal convergence of water vapor ( $\text{mm h}^{-1}$ );  $Z$  is the vertical convergence of water vapor ( $\text{mm h}^{-1}$ ), which is zero after vertical integral over the whole air column;  $E$  is evaporation from the ocean surface and from rain ( $\text{mm h}^{-1}$ );  $P$  is precipitation ( $\text{mm h}^{-1}$ ); and  $C$  is liquid and solid water stored as cloud ( $\text{mm h}^{-1}$ ). For simplicity, we refer to  $C$  as cloud storage.<sup>1</sup> Please note that the total of  $P$  and  $C$  is condensation and deposition.

The local change of water vapor [left-hand-side term in (1)] is computed from the vertical integral of the local change of the mixing ratio:

$$\frac{\partial(\text{TPW})}{\partial t} = \frac{1}{g} \int_{p_2}^{p_1} \frac{\partial q}{\partial t} dp, \quad (2)$$

where  $q$  is the water vapor mixing ratio, and  $p_1$  and  $p_2$  are the pressure levels bounding the model layers in which the integrations are carried out. A leapfrog differencing technique was used to solve the time derivative.

The horizontal moisture flux convergence can be calculated from the vertical integral of the convergence of the water vapor flux over all vertical layers in the column:

$$F = -\frac{1}{g} \int_{p_2}^{p_1} \nabla \cdot (q\mathbf{V}) dp, \quad (3)$$

where  $\mathbf{V}$  is the horizontal velocity vector. A centered finite-difference scheme was used.

Evaporation from the ocean surface (we neglect evaporation from rain and the limitation of this simplification will be discussed in section 4b) is estimated from a bulk parameterization method described in Liu (1988):

$$E = \rho C_E U (q_s - q) = \rho C_E U \Delta q, \quad (4)$$

where  $\rho$  is the density of the surface air,  $q_s$  is the saturated mixing ratio at the sea surface temperature (SST), and  $U$  and  $q$  are the wind speed and mixing ratio in the bottom model layer. In addition,  $C_E$  is the drag coefficient for the moisture exchange, and  $\Delta q$  is the sea surface – air moisture difference. The drag coefficient is stability dependent and is computed following the time-implicit Louis surface flux parameterization method used in the NOGAPS physics package and described in Louis (1979).

The precipitation rate is obtained from the MPA-RT product, which is averaged or interpolated to the NOGAPS  $1^\circ \times 1^\circ$  latitude–longitude grid with a 12-h time step for the water budget calculations. The cloud storage term is calculated as a residual.

### 2) VERTICAL WIND SHEAR

Many studies have shown that the vertical wind shear could hinder convective growth and storm intensification (Rodgers et al. 1994; Zehr 2003). However, Molinari et al. (2004) demonstrated that vertical shear of  $5\text{--}10 \text{ m s}^{-1}$  actually produced downshear convective outbreaks that were favorable to the storm development of Hurricane Danny (1997). In this study, vertical wind shear is examined to see how it interacts with the storm to yield intensity and rainfall changes for Isidore and Lili. The presence of shear also leads to an asymmetric distribution of precipitation in tropical cyclones (Lonfat et al. 2004; Halverson et al. 2006). The vertical wind shear within 1000 km of the tropical cyclone is derived from the 850- and 200-mb NOGAPS wind analyses. The large domain is used because the maximum storm size of Isidore was a 1100-km radius (Lili's maximum storm size was about 800-km radius). The horizontal winds are averaged over the domain at the 850- and 200-mb levels to derive a mean environmental wind vector at each level. The vertical shear is then estimated from the magnitude of the difference between the mean wind vectors at 850 and 200 mb.

### 3) SEA SURFACE TEMPERATURE

To determine whether the SSTs are warm enough (i.e.,  $\text{SST} > 26^\circ\text{C}$ ) to allow for sufficient moist static

<sup>1</sup> Please note it is not the storage term in the cloud content budget equation, which is simply the local change of cloud liquid water and ice.

energy flux to support convection in Hurricanes Isidore and Lili, mean SSTs within a 1000-km radius of the tropical cyclone are derived from NOGAPS analyses of the surface skin temperature. The domain is chosen for the same reason as for the vertical wind shear.

#### 4) ANALYSIS METHOD

The water budget parameters are derived in storm-relative coordinates with an evaluation domain of  $12^\circ$  radius from the storm circulation center. The storm total volumetric TPW and water budget terms including MPA-RT rain rate are derived from the integrals in regions inside the tropical cyclone. The storm size (i.e., the maximum storm radius) as a function of time is determined from the MPA-RT rainfall images. A combination of automatic and manual methods is used to draw a circle around the storm at the observation time by excluding rain that is not associated with the tropical cyclone (H. Pierce 2005, personal communication). Only pixels inside the circle of the maximum storm radius and are counted when calculating the total volumetric parameters ( $\sum X$ ):

$$\sum X = \sum_{i=0}^{i=n} X_i A, \quad (5)$$

where  $X$  represents any of the TPW and water budget parameters,  $A$  is the area of each single pixel ( $1^\circ \times 1^\circ$ ), and  $n$  is the number of data points inside the storm.

The azimuthally mean values are calculated in 111-km-wide (about  $1^\circ$  radius) annuli around the storm center outward to the 1111-km radius. The resulting dataset allows us to examine the radial dependence of parameters as a function of time. Inner-core [within 111 km of the tropical cyclone; Rodgers et al. (1994)] mean parameters can also be computed as the storm evolves.

### 3. TRMM-based combined radar-radiometer IWP and LWP estimates

Figure 1 shows the plan view of TRMM-based combined TMI and PR estimates of IWPs and LWPs for Isidore's TRMM overpass at 1130 UTC 21 September and Lili's TRMM overpass at 0600 UTC 2 October 2002. TMI 85-GHz polarization-corrected temperature (PCT) 240-K contours are overlaid in the figure to indicate the ice scattering signature of the cloud. A detailed definition of PCT can be found in Spencer et al. (1989). PCT is used instead of the brightness temperature to allow discrimination between low brightness temperatures due to the radiometrically cold sea surface versus those due to precipitation. TRMM had 21 (18) overpasses for Isidore (Lili), but only these two

overpasses were directly sampled by the TRMM PR while the major part of the storm was over ocean, which are the requirements for the combined radar-radiometer algorithm (Jiang and Zipser 2006). Fortunately, during these two overpasses, Isidore and Lili were over the same location (Yucatan Strait) and in same intensity stage (maximum surface wind speed of 100 kt, category 3). Therefore, the water path estimates derived from these two overpasses for Isidore and Lili are comparable.

From Fig. 1, both the IWP and LWP of Isidore are much larger than those of Lili for these two overpasses. To quantify the differences, Table 1 gives the comparison of the storm mean IWP and LWP during these TRMM overpasses. The mean IWPs (LWPs) for Isidore and Lili are 1.94 (2.39) and 0.81 (1.45) mm, respectively. As presented in Jiang (2004), the mean IWPs (LWPs) for the inner-core convective region and outer rainband stratiform region for one TRMM overpass of Hurricane Isabel (2003) are 3.59 (2.83) and 3.02 (1.66) mm, respectively. Isabel was a category 5 hurricane, so the retrievals show that there is a lot more ice in Isabel than there is in Isidore and Lili. As for the liquid water, Isidore's (Lili's) LWP amount is similar to that in the convective (stratiform) region of Isabel. The mean IWP (LWP) for Isidore was a factor of 2.5 (1.5) higher than that for Lili. However, since the cloud storage term in (1) includes the time change of both precipitation water content (from larger size cloud particles) and cloud water content (from smaller size cloud particles), and the TRMM-based combined radar-radiometer algorithm could only retrieve the precipitation water content, the results should be used with caution. An approximate estimate of storm total precipitation water mass is also made from the retrieval and is presented in Table 1. Based on the  $C$  (condensation excluding precipitation) values (the average is about  $1.0 \text{ km}^3 \text{ h}^{-1}$  for Isidore and  $0.4 \text{ km}^3 \text{ h}^{-1}$  for Lili) shown in the next section (Fig. 4), it would take about 1 h for the water vapor source only to establish the observed storm total water mass, which is  $0.7 \text{ km}^3$  for Isidore and  $0.4 \text{ km}^3$  for Lili. In reality, there are other sources for the total condensation.

### 4. Water budget of Isidore and Lili

#### a. Comparison of SSM/I-derived and NOGAPS-derived total precipitable water (TPW)

Although the SSM/I-observed TPW has been assimilated into NOGAPS, the fidelity of the assimilation depends on many factors. To examine the performance of the assimilation strategy of NOGAPS analyses, the spa-

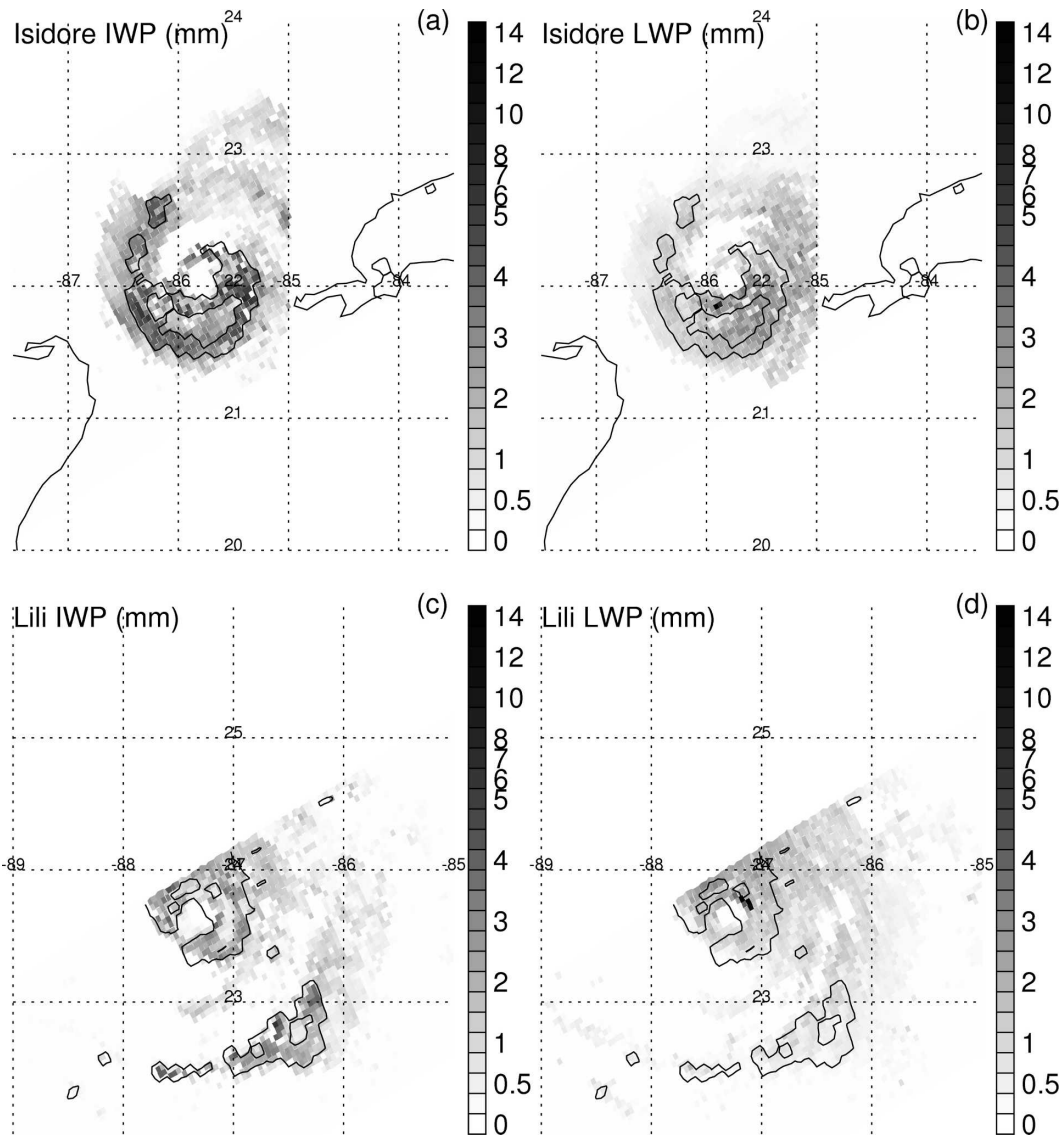


FIG. 1. Plan view of TRMM-based combined TMI and PR estimates of Isidore's (a) IWP and (b) LWP on 21 Sep and Lili's (c) IWP and (d) LWP on 2 Oct 2002. TMI 85-GHz PCT 240-K contours are indicated as solid lines. See text for definition of PCT.

tial distributions of the total precipitable water (TPW) observed from SSM/I and derived from the NOGAPS analyses (vertical integral of mixing ratio) at approximately 1200 UTC 23 September and 0000 UTC 24 Sep-

tember 2002 for Isidore and 1200 UTC 2 October and 0000 UTC 3 October 2002 for Lili are shown in Figs. 2 and 3, respectively. It is seen from the figures that the SSM/I-derived and the NOGAPS-analyzed synoptic-scale TPW fields are generally similar. However, there are some subtle small-scale differences caused either by differences in time and resolution of the products or the inability of the SSM/I to observe TPW over land and in raining areas. Nevertheless, since the NOGAPS-analyzed TPW is consistent with the large-scale features observed by the SSM/Is over the Gulf of Mexico, the water budget derived from NOGAPS analyses and MPA-RT rain estimates is calculated to determine the

TABLE 1. Mean IWP and LWP and storm total water mass derived from the TRMM combined radar-radiometer estimates for the Isidore and Lili TRMM overpasses as shown in Fig. 1.

	Mean IWP (mm)	Mean LWP (mm)	Storm total ice + liquid water mass (km <sup>3</sup> )
Isidore	1.94	2.39	0.7
Lili	0.81	1.45	0.4

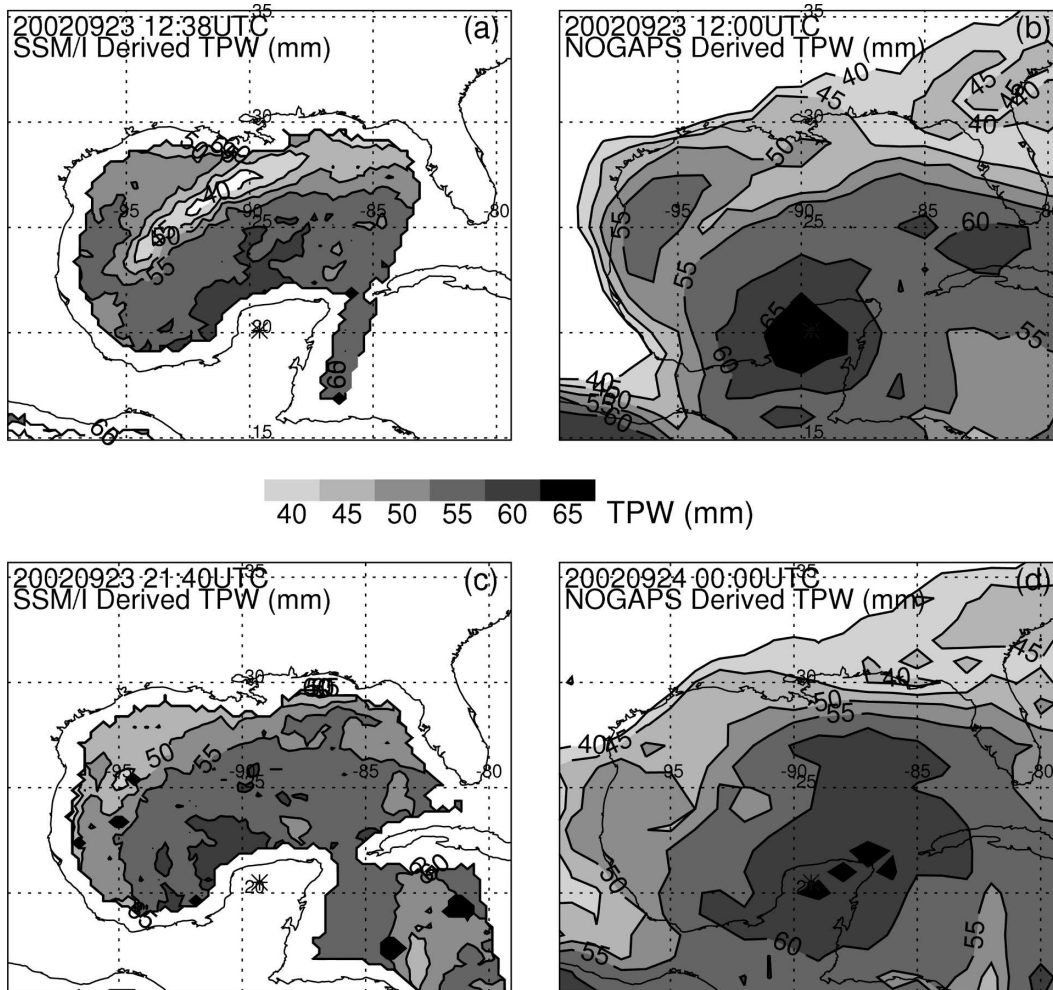


FIG. 2. The (left) SSM/I-observed and (right) NOGAPS-derived environmental TPW (mm) at approximately (top) 1200 UTC 23 Sep and (bottom) 0000 UTC 24 Sep 2002 for Isidore.

crucial environmental factors that initiated and maintained the large difference of rainfall before and during the landfalls of Isidore and Lili.

#### *b. Time series of volumetric water budget parameters*

The time series of storm total volumetric water budget parameters, including horizontal moisture convergence, precipitation (MPA-RT rain), evaporation, local change of TPW, and cloud storage, for Isidore and Lili are given in Fig. 4. In the water budget calculation, to match the NOGAPS-derived parameters, MPA-RT rains have been averaged into a  $1^\circ \times 1^\circ$  latitude-longitude spatial resolution and only 0000 and 1200 UTC times of MPA-RT data are used. Although the calculation has been degraded to low spatial and temporal resolutions, those total volumetric rain episodes identified in Fig. 7 of Part I for Isidore and Lili can still

be seen in Fig. 4. A positive aspect of this degradation is that it smoothes out artifacts in the 3-hourly MPA-RT data induced by the data source shifting from IR to microwave satellite observations (G. Huffman and H. Pierce 2005, personal communication).

It is seen clearly from Fig. 4 that the moisture convergence was the dominant term and contributed most of the total rain for Isidore. This is also the case for Lili. Evaporation was the second largest contributing term, while the local change of TPW was negligible. During the second total rain episode of Isidore between 22 and 25 September as described in section 4a of Part I, the cloud storage term is comparable with the MPA-RT rain, indicating low precipitation efficiency (about 50%). This period was coincident with Isidore's size expanding. The large cloud storage term indicates the cloud mass increase. When Isidore made landfall on 26–27 September, the precipitation term was larger

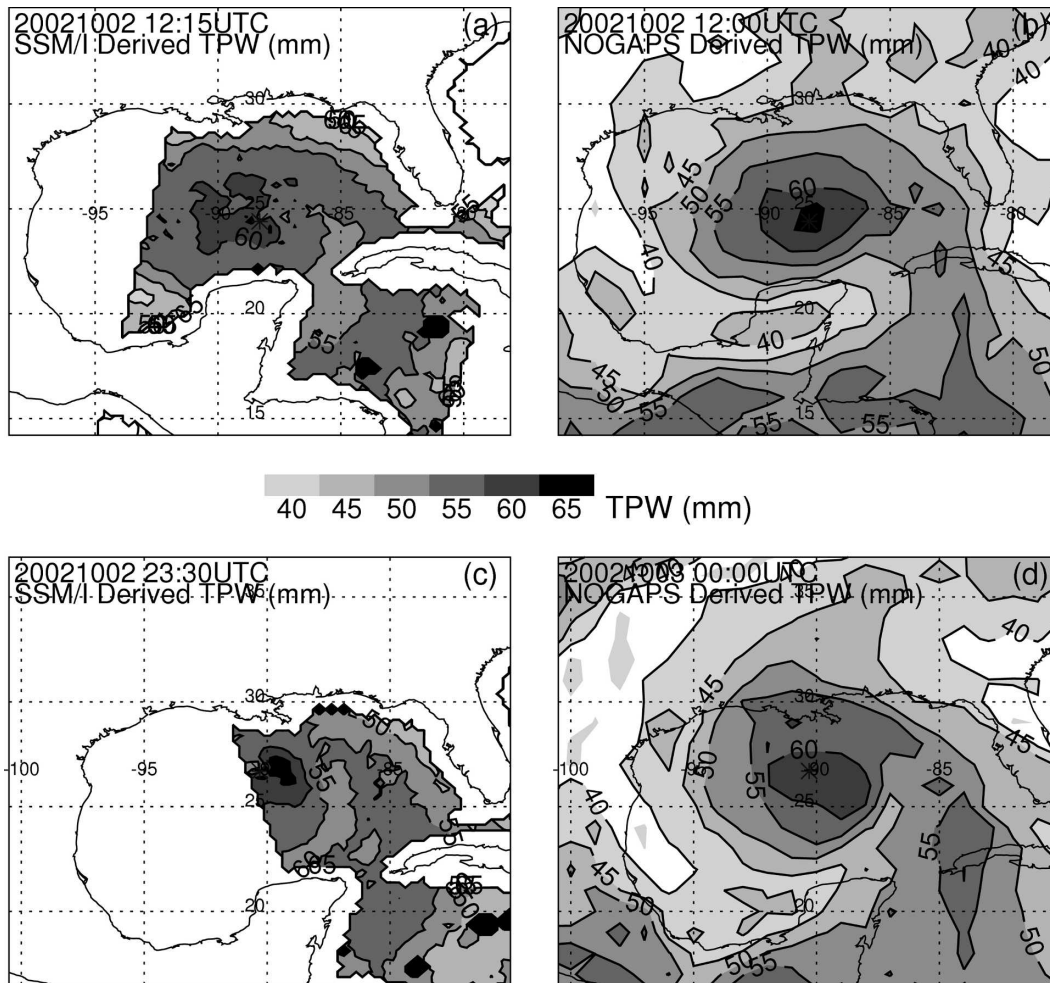


FIG. 3. Same as in Fig. 2, but for Lili.

than the moisture convergence term again. During landfall, the differences between precipitation and the moisture convergence term were balanced by the large negative value of the cloud storage term and the local change of TPW. Since the cloud storage is calculated as a residual and evaporation from rain and cloud is neglected in the water budget balance, the negative value of the residual term indicates evaporation from rain and cloud.

Table 2 gives the 12.5-day temporal integral of the storm total volume of the water budget parameters between 0000 UTC 15 September and 0000 UTC 27 September for Isidore and between 0000 UTC 22 September and 0000 UTC 4 October for Lili. All of the terms for Isidore are about a factor of 2.5 larger than those of Lili, except for the local change of TPW. After averaging for almost the entire lifetime of each storm, the horizontal moisture convergence contributed about 53% (53%) of the storm total condensation (or the

total of the horizontal moisture convergence and ocean flux) and the ocean surface moisture flux contributed about 47% (52%) of that for Isidore (Lili). Again, the dominant terms are the moisture convergence and precipitation for both storms. This is similar to results found in previous studies (Spar 1953; Bradbury 1957; Kurihara 1975; Carr and Bosart 1978; Gamache et al. 1993; Braun 2006). The contribution of the ocean moisture flux is substantial. Hawkins and Rubsam (1968) examined budgets of Hurricane Hilda (1964) in its intensifying stage using aircraft observations. They found that the ocean moisture source inside an 80-km radius was approximately 54% of the total moisture import below 600 mb and crossing that radius. A similar study of a much stronger storm (Hurricane Inez 1966) by Hawkins and Imbembo (1976) produced comparable results. Gamache et al. (1993) calculated a water vapor budget for Hurricane Norbert (1984) and suggested that about 40% of the vapor converging into the vol-



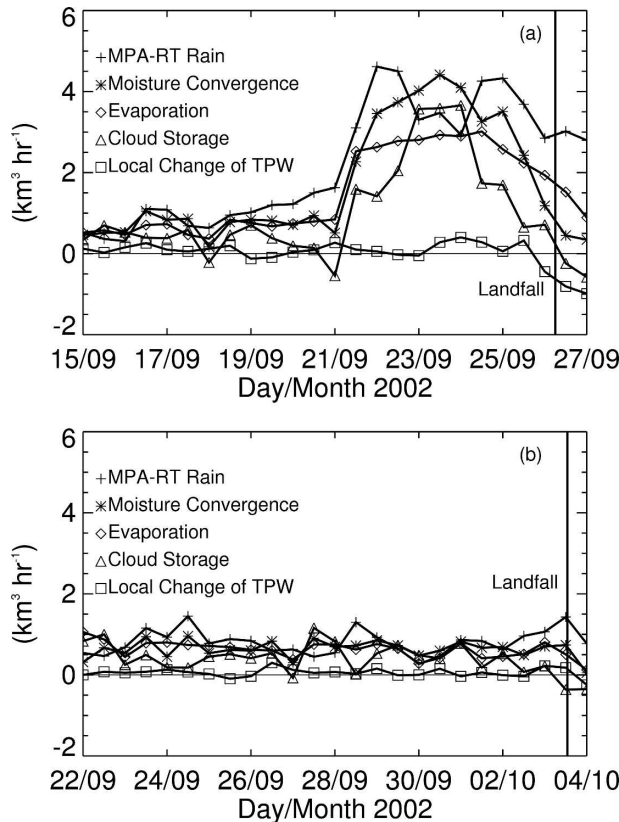


FIG. 4. Time series of storm volumetric water budget parameters derived from 12-h NOGAPS analysis and MPA-RT product for (a) Isidore (15–27 Sep 2002) and (b) Lili (22 Sep–4 Oct 2002). The vertical lines indicate landfall times of Isidore and Lili.

ume was from the ocean moisture flux. However, Braun (2006) found that the ocean moisture flux is only about 8% of the total moisture convergence into the 200-km-radius volume for Hurricane Bonnie (1998) by using a high-resolution model simulation. Braun (2006) claimed that observation-based studies by Hawkins and Rubsam (1968), Hawkins and Imbembo (1976), and Gamache et al. (1993) generally overestimated the role of the ocean source. In fact, our results are consistent with the observational and modeling studies by Malkus

TABLE 2. The 12.5-day integral of the storm total volume of the water budget parameters between 0000 UTC 15 Sep and 0000 UTC 27 Sep for Isidore and between 0000 UTC 22 Sep and 0000 UTC 4 Oct for Lili (see text for details).

Volume ( $\text{km}^3$ )	Isidore	Lili
MPA-RT rain	661	241
Moisture convergence	506	191
Evaporation	447	186
Cloud storage	287	120
Local change of TPW	5	16

and Riehl (1960), Kurihara (1975), and Braun (2006). Their results showed that the ratio of the ocean moisture flux to the total condensation increases from 8% for the integrated volume being a 200-km radius to 20% for the integrated volume being a 500-km radius. In this study, the integrated volume is about  $8^\circ$ – $12^\circ$  radius for Isidore and  $6^\circ$ – $8^\circ$  radius for Lili. Compared to the hurricane's inner region, the large outer region that we integrated has a relatively smaller wind speed convergence and, therefore, smaller moisture convergence. So the relative contribution of the ocean moisture flux to the total condensation has to be larger. The local change of the TPW term was negligible for both storms. About 70% (67%) of the condensate falls to the surface as precipitation for Isidore (Lili). This is as same as that found in Braun (2006). The cloud storage term is about a factor of 2.5 larger than that of Lili. This is confirmed from the TRMM combined radar and radiometer estimation shown in section 3. Based on this estimate, the total precipitation cloud ice and liquid water mass was about  $0.7 \text{ km}^3$  for Isidore's TRMM overpass on 21 September, but was only  $0.4 \text{ km}^3$  for Lili's TRMM overpass on 2 October (Table 1). However, this estimate is only based on one TRMM snapshot and may not be able to completely explain the difference of a 12.5-day integration.

Although the local change in the TPW is very small, the TPW parameter itself is related to the horizontal moisture convergence term and indicates how moist the storm environment is. Figure 5 presents the comparison of Isidore and Lili's volumetric TPW and rain as a function of time. Starting at 21 September, Isidore's volumetric TPW abruptly increased, which occurred simultaneously with the second storm total rain episode. The storm volumetric TPW increased approximately from

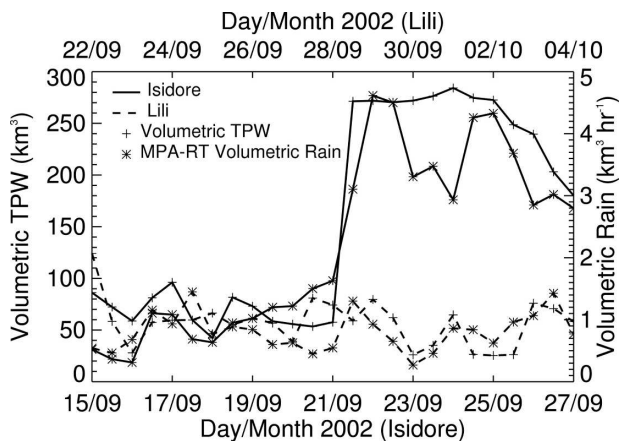


FIG. 5. Comparison of the volumetric TPW and rain for Isidore (15–27 Sep 2002) and Lili (22 Sep–4 Oct 2002) as a function of time.

50 to 275 km<sup>3</sup> while the storm total volumetric rain increased from 1.5 to 4.5 km<sup>3</sup> h<sup>-1</sup> (see section 4a of Part I). Both the expansion of the storm and its intensification contributed to these large increases in rain volume (see Figs. 5 and 6 in Part I). Most importantly, the storm's environment became much moister. Isidore's volumetric TPW continued to be above 220 km<sup>3</sup> until 26 September. After Isidore made landfall, the storm volumetric TPW decreased to 170 km<sup>3</sup> on 27 September. Lili's volumetric TPW was much smaller. The maximum value was about 90 km<sup>3</sup> on 24 September and 3 October.

### c. Radial-time distribution of water budget parameters

To delineate the time change in the radial distribution of Isidore and Lili's water budget parameters, the rain rate, moisture convergence, evaporation, local change of TPW, cloud storage, and TPW are azimuthally averaged to within 10 annuli, 111 km in width, extending outward from storm centers and displayed with time in Figs. 6 and 7 for Isidore and Lili, respectively.

After averaging over a large surface area, the degraded azimuthally averaged rain rates shown in Figs. 6a and 7a are able to better define rain episodes than the high-resolution plots given in Fig. 8 of Part I. Isidore's four rain episodes (16–17, 19–23, 24–25, and 26–27 September) can be identified from Fig. 6a and are matched with those seen from Fig. 7 of Part I. The radial distribution of Isidore's horizontal moisture convergence (Fig. 6b) resembles the pattern of the radial distribution of Isidore's rain (Fig. 6a). During 16–17 September, the moisture convergence reached its first maximum of 1.5 mm h<sup>-1</sup> around the inner-core region while the rain (TPW; Fig. 6f) maximum was 2 mm h<sup>-1</sup> (60 mm) during the same period and over the same regions. No obvious maxima were seen in the evaporation plot (Fig. 6c) in this period. The second maximum (8 mm h<sup>-1</sup> of moisture convergence, 10 mm h<sup>-1</sup> of rain, 1.5 mm h<sup>-1</sup> of evaporation, and 70 mm of TPW) occurred on 22 September. During this second episode, the outer contours of 0.5 mm h<sup>-1</sup> rain, moisture convergence, and evaporation extended up to 1111-km radius from Isidore's circulation center. The 55-mm TPW contour extended to a 777-km radius. The third (24–25 September) and fourth (26–27 September) episodes were clearly seen in rain and moisture convergence plots, but they appeared to be merged into only one episode in the evaporation and TPW plots. From Fig. 6f, the TPW increased dramatically on 21 September. The 65-mm contour of TPW during 21–27 September extended to about a 333-km radius, indicating a large area of environmental moisture that is crucial to Isi-

dore's torrential rain during its landfall. It is interesting to note that during 26–27 September, the local change of TPW (Fig. 6e) had a minimum value of -0.7 mm h<sup>-1</sup>, which means that the local TPW value decreased and the decreased amount was contributed to the heavy rain during Isidore's landfall. In addition, the large area of positive values of cloud storage (Fig. 6d) during 22–25 September was located between 555- and 1111-km radius. It is consistent with the above discussion that the size expansion of Isidore is the main reason for the cloud storage increase.

Two total rain episodes of Lili on 24 September and 3 October can be seen in Fig. 7a. One of Lili's convective bursts on 1 October can also be seen in this low-resolution contour plot. From Figs. 7b, 7c, and 7f, we see that Lili experienced strong moisture convergence and ocean surface moisture flux during 1–4 October. The TPW maximum reached 65 mm during this period, but the 65-mm contour only covered up to a 200-km radius over intermittent time periods. During Lili's lifetime, the 55-mm TPW contour never extended beyond 500-km radius and the TPW maximum never reached 70 mm, showing that Lili's environment was much drier than Isidore's. During Lili's landfall, the local decrease of TPW (Fig. 7e) was also much weaker than that experienced by Isidore. Similar to Isidore, Lili's cloud storage (Fig. 7d) was positive (indicating cloud mass increase) when the storm was over ocean during 27 September–2 October and was negative (indicating evaporation from rain and cloud) during the storm's landfall on 3 October.

From a TPW perspective, Isidore was embedded in an inherently much wetter environment than Lili. This is the major reason why Isidore's moisture convergence was much larger than Lili's. However, the storm's wind field is also a factor that influences the magnitude of the moisture convergence. To examine these processes in more detail, the moisture convergence term is partitioned into two components,  $q\nabla \cdot \mathbf{V}$  and  $\mathbf{V} \cdot \nabla q$ , to see the relative importance of them. It is found that the magnitude of moisture convergence is dominant by the first component. From the horizontal contours of wind and the mixing ratio (not shown here), we see that both the mixing ratio and divergence of the wind field are much larger for Isidore during 22–24 September than those of Lili during anytime of Lili's life cycle. During the period of 22–24 September, Isidore was interacted with the Yucatan and also reached its maximum intensity. This fact indicates that the frictional convergence, the storm's strong intensity, and its TPW increase are the main factors that caused the large moisture convergence. The ocean surface moisture flux (evaporation) is the second contributor to rain. The sea surface - air

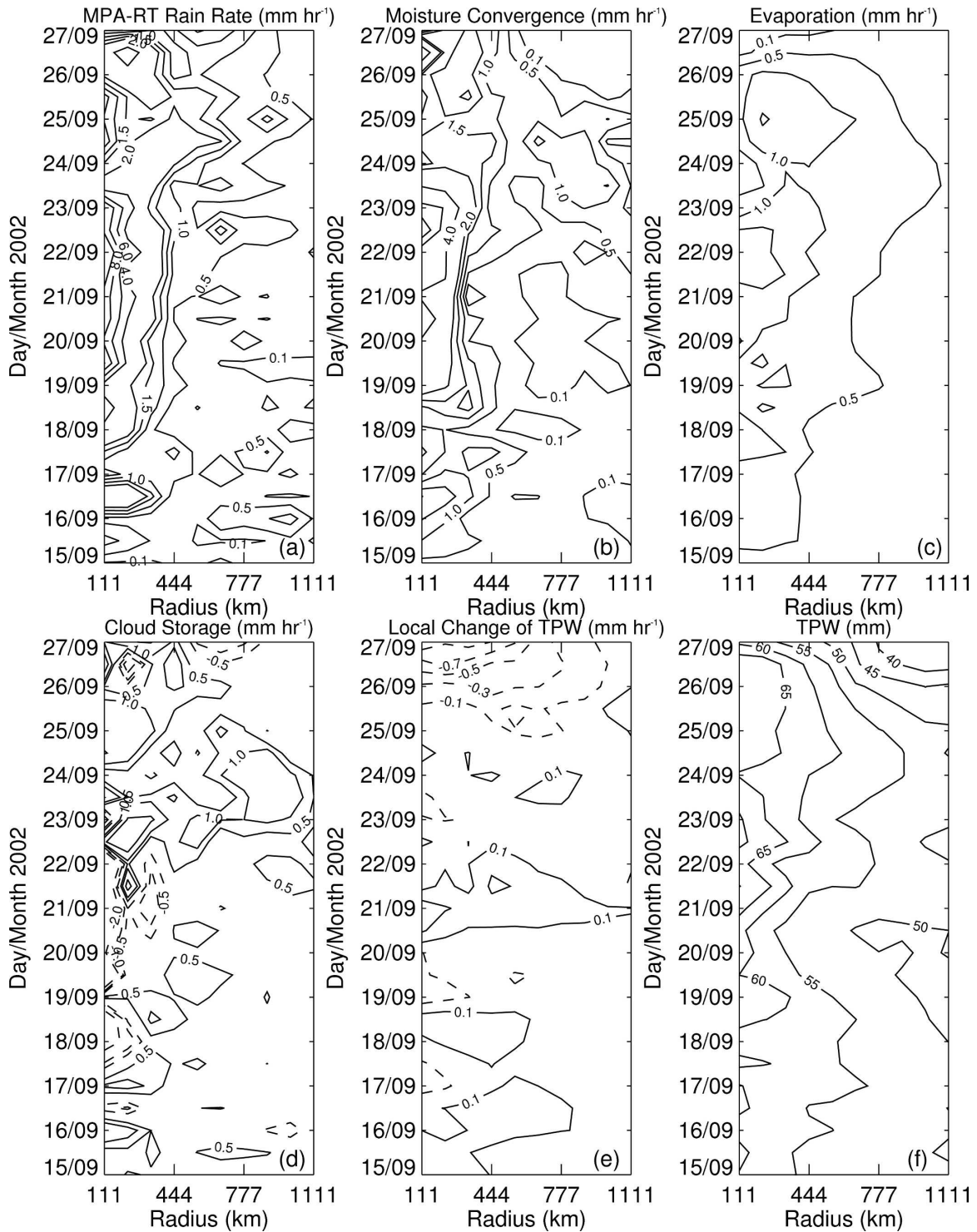


FIG. 6. Time-radius view of Isidore's azimuthally averaged (a) rain rates derived from the MPA-RT product, (b) horizontal moisture convergence, (c) evaporation, (d) cloud storage, (e) local change of TPW, and (f) TPW for every 12 h. Here, (b),(e),(f) are derived from NOGAPS analyses, and (c) is derived as the water budget residual. Parameters are azimuthally averaged for annuli 111 km in width extending 1111 km outward from the center.

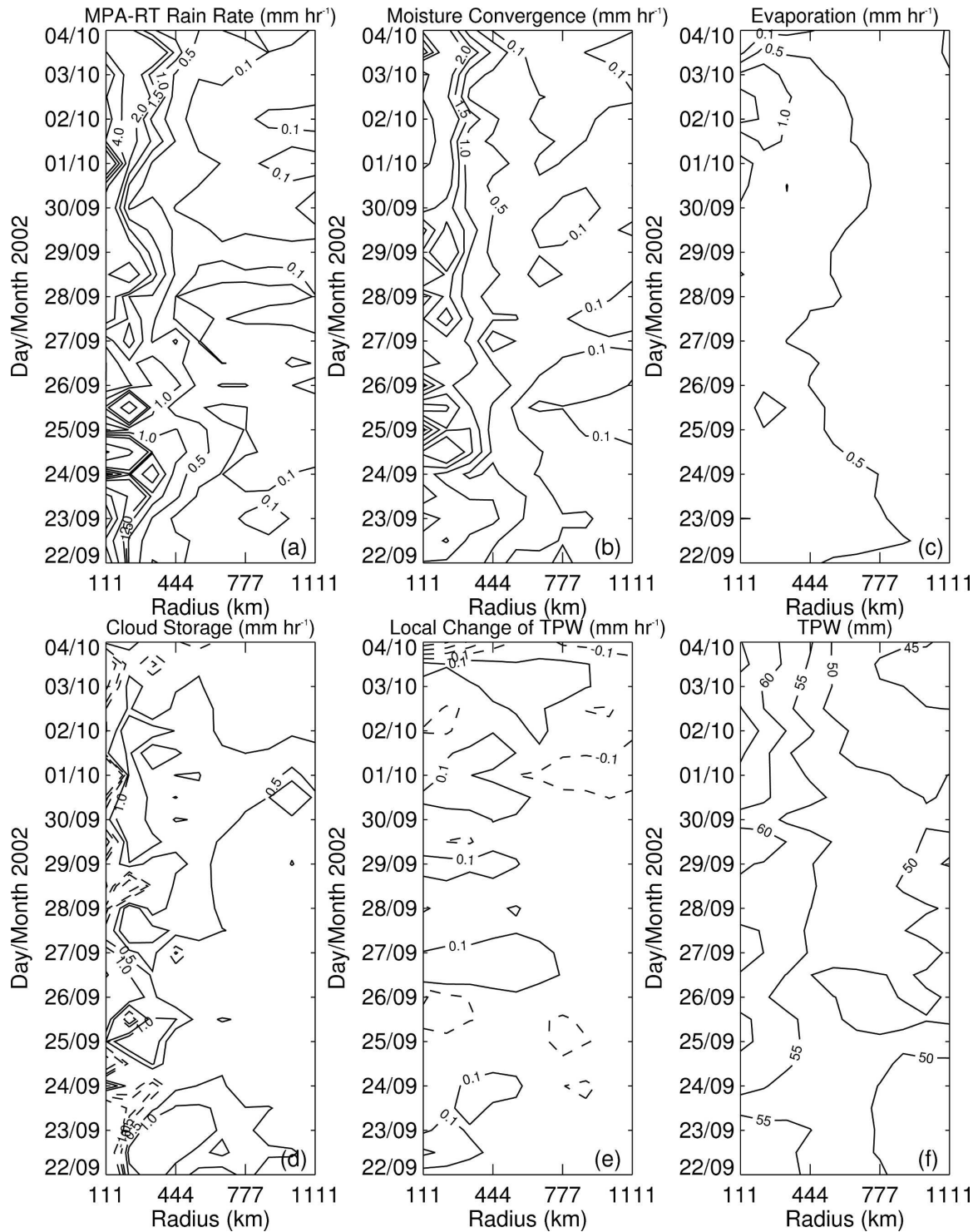


FIG. 7. Same as in Fig. 6 but for Lili.

moisture difference ( $\Delta q$ ) and the storm's near-surface horizontal wind speed are the two major factors in terms of evaporation. To understand why Isidore's evaporation was much larger than Lili's, these two fac-

tors need to be carefully examined. The wind factor will also help us understand the moisture convergence difference between Isidore and Lili.

Figures 8 and 9 show the time-radius plots of the

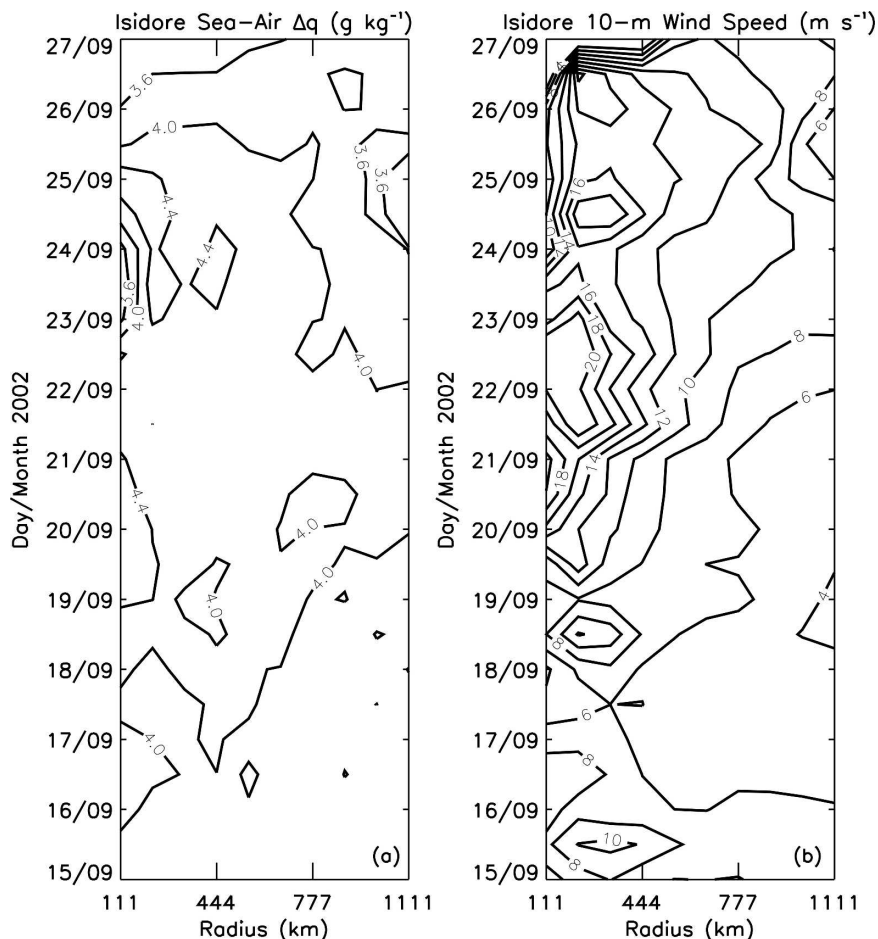


FIG. 8. Time-radius view of Isidore's azimuthally averaged (a) sea surface - air  $\Delta q$  ( $\text{g kg}^{-1}$ ) and (b) 10-m wind speed derived from NOGAPS analyses. Parameters are azimuthally averaged for annuli 111 km in width extending 1111 km outward from the center.

azimuthally averaged sea surface - air  $\Delta q$  and horizontal wind speed at 10 m above the surface (10-m wind speed) derived from NOGAPS analyses for Isidore and Lili, respectively. Generally, it is seen from Figs. 8 and 9 that Isidore's 10-m wind was stronger than Lili's. The 10  $\text{m s}^{-1}$  wind speed contour for Isidore (Lili) extended out to 888-km (only 444 km) radius. The sea surface - air  $\Delta q$  maxima for Isidore were larger than those for Lili by about 0.2-0.4  $\text{g kg}^{-1}$ . From Fig. 6c, Isidore's evaporation had two episodes (defined as evaporation equal or greater than 1.5  $\text{mm h}^{-1}$ ): one on 20-23 September and one on 24-26 September. Compared with Figs. 8a and 8b, these two episodes were approximately coincident with the sea surface - air  $\Delta q$  maxima on 19-22 September (4.4  $\text{g kg}^{-1}$ ) and 23-25 September (4.6  $\text{g kg}^{-1}$ ) and the 10-m wind maxima on 21-23 September (20  $\text{m s}^{-1}$ ) and 24-26 September (18  $\text{m s}^{-1}$ ). From Fig. 7c, Lili's evaporation had only one episode on 2-3 October and its covered area was much less than

Isidore's first evaporation episode. Compared with Figs. 9a and 9b, during this episode the sea surface - air  $\Delta q$  maximum was only 3.9  $\text{g kg}^{-1}$  and the 10-m wind maximum was 18  $\text{m s}^{-1}$ .

## 5. Other environmental parameters

### a. Vertical wind shear

The evolution of Isidore and Lili's storm total volumetric rain and the mean 12-h change in the 850-200-mb environmental vertical wind shear is shown in Fig. 10. Isidore encountered moderate vertical wind shear before 26 September (i.e., mean value of 6.4  $\text{m s}^{-1}$ ). However, on 18-20 September, the vertical wind shear increased from 3 to 11  $\text{m s}^{-1}$  during a 2-day period. Then from 20 to 23 September, the vertical wind shear decreased from 11 to 4  $\text{m s}^{-1}$  and the low shear continued to 25 September. During this low-shear period, Isidore's volumetric rain reached a maximum. On 26 Sep-

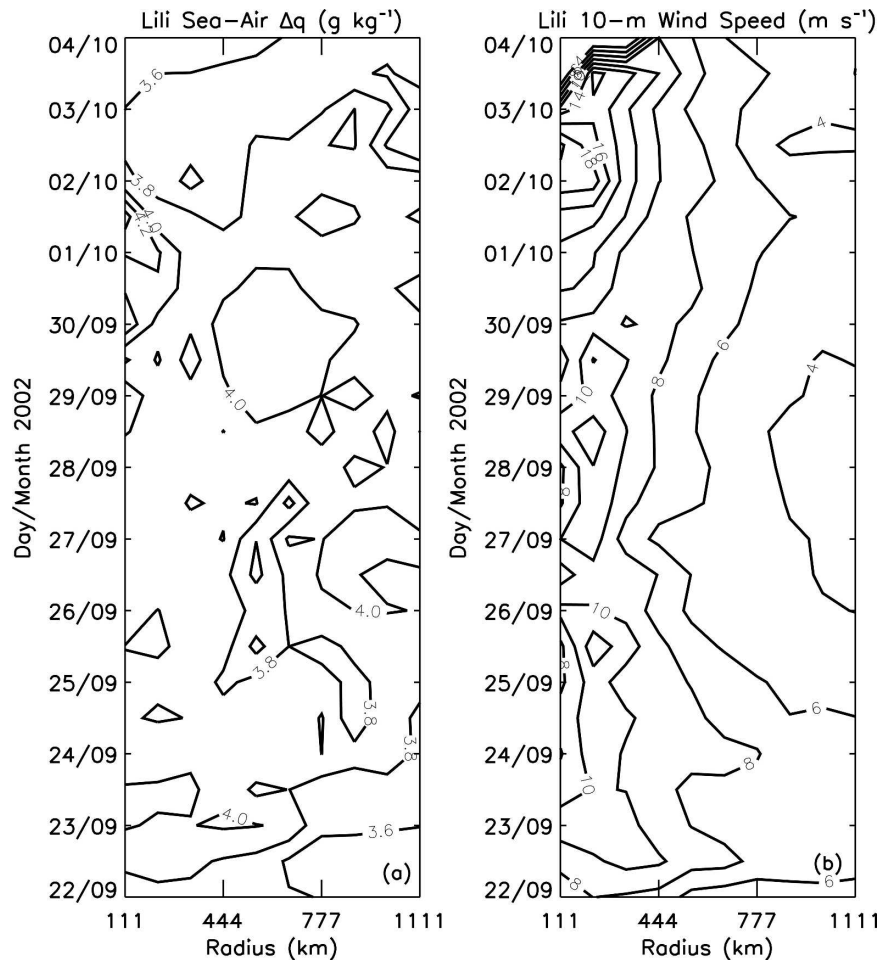


FIG. 9. Same as in Fig. 8 but for Lili.

tember, Isidore began to move close to a midtropospheric trough as mentioned in section 3 and the vertical wind shear abruptly increased from 4 to  $17 \text{ m s}^{-1}$ . During Isidore's landfall, the shear values were larger than the threshold value of  $10 \text{ m s}^{-1}$  needed to inhibit the production of rainfall (Rodgers et al. 1994; Rodgers and Pierce 1995). As a result, the storm volumetric rain decreased during Isidore's landfall but was still quite large ( $3 \text{ km}^3 \text{ h}^{-1}$ ) due to the strong moisture convergence and decreasing cloud storage effects as discussed in section 4.

Lili encountered moderate vertical wind shear during its lifetime (i.e., maximum value of  $12 \text{ m s}^{-1}$  and mean value of  $5.7 \text{ m s}^{-1}$ ). Generally, Lili's shear decreased steadily throughout its lifetime until the trough interaction. On 28 September, the vertical wind shear reached an extremely low value of  $0.2 \text{ m s}^{-1}$ , consequently, Lili's storm total volumetric rain had a secondary peak on that day. A second minimum shear value of

$1.8 \text{ m s}^{-1}$  on 1 October appeared to have helped the convective burst on that day.

#### b. Sea surface temperature

The time evolution of SSTs in the path of Isidore and Lili is shown in Fig. 11. Both Isidore and Lili encountered SSTs above  $28^\circ\text{C}$ , which is greater than the critical temperatures required to support convective growth [i.e., approximately  $26^\circ\text{C}$ ; Gray (1979)] during these two storms' lifetimes. However, generally Isidore's SSTs were larger than Lili's. The figure also indicates an increase in the SSTs of nearly  $1.0^\circ\text{C}$  between 18 and 21 September as Isidore moved northwestward to a warm SST area and Isidore's SST reached nearly  $29.5^\circ\text{C}$  on 21 September. This explains the large increase in TPW for Isidore on 21 September. After 21 September, Isidore's SSTs slowly decreased and reached their minimum of  $28.2^\circ\text{C}$  at 0000 UTC 27 September, when most of the storm was over land. Al-

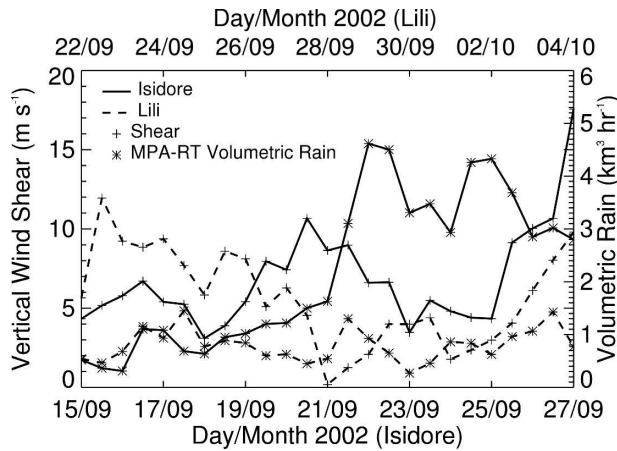


FIG. 10. The time change of the averaged vertical wind shear ( $\text{m s}^{-1}$ ) that Isidore and Lili encountered and the MPA-RT-derived storm total volumetric rain ( $\text{km}^3 \text{h}^{-1}$ ).

though SSTs were warm enough to maintain convective growth during Isidore's lifetime, it is obvious that the increase and decrease of SSTs, respectively, between 18 and 21 September and after 21 September had a profound effect on Isidore's intensity.

Lili's SSTs remained between  $28.5^\circ$  and  $29^\circ\text{C}$  throughout the majority of her lifetime. Note that the SSTs were abruptly increased from  $28.1^\circ$  to  $28.9^\circ\text{C}$  between 22 and 24 September. During this period, a convective burst occurred and Lili's storm total volumetric rain reached its first local maximum. Following a decrease during 24–25 September, Lili's SSTs slowly increased to nearly  $29^\circ\text{C}$  on 30 September and decreased a little to  $28.8^\circ\text{C}$  on 1 October. Note that the second convective burst was on 1 October. After that day, the SSTs continued to decrease slowly and this decrease

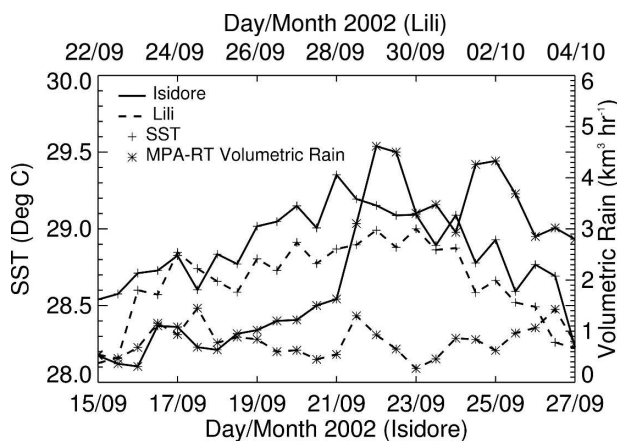


FIG. 11. The time change of the averaged SST ( $^\circ\text{C}$ ) within 1000 km from the storm center for Isidore and Lili and the MPA-RT-derived storm total volumetric rain ( $\text{km}^3 \text{h}^{-1}$ ).

appeared to have had little influence on Lili's rapid intensification on early 3 October.

### c. Near-surface $\theta_e$

To illustrate the heat and moisture capacity of the storm, the near-surface equivalent potential temperatures  $\theta_e$ 's are estimated from NOGAPS analyses. Figure 12 gives the time–radius view of Isidore and Lili's azimuthally averaged near-surface  $\theta_e$  for annuli 111 km in width extending 1111 km outward from the center. The figure suggests that the near-surface  $\theta_e$  had an effect on Isidore and Lili's intensity and rainfall production. During 21–23 September, the double peak in near-surface  $\theta_e$  ( $352 \text{ K}$ ) around Isidore's inner-core regions is associated with dramatically increased storm intensity and storm volumetric rain. For Lili, the rapid intensification on 3 October was clearly associated with a near-surface  $\theta_e$  maximum ( $344 \text{ K}$ ), which indicates large near-surface heat and moisture energy and an increased likelihood of deep convection.

### d. Upper-tropospheric divergence

The time evolutions of the inner-core mean 150-mb divergence ( $10^{-5} \text{ s}^{-1}$ ) and the MPA-RT-derived inner-core mean rain rate ( $\text{mm h}^{-1}$ ) for Isidore and Lili are presented in Fig. 13. The figure indicates that the inner-core mean upper-tropospheric divergence was well correlated with the inner-core mean rain rate for both Isidore and Lili. This finding is consistent with previous studies that showed the upper-level outflow is important for tropical cyclone intensification. This result is obtained from the low-resolution NOGAPS analyses that only allows us to resolve a few (one to four) data points for inner-core regions. Therefore, this good correlation supports the hypothesis that the 150-mb divergence can be a proxy for convective intensity, which is related to storm intensity. This is also evidence of the usefulness of the analyses from the NOGAPS model.

## 6. Summary

Combined with the 3-hourly real-time Goddard Multisatellite Precipitation Analysis (MPA-RT) product, the NOGAPS analyses are used to evaluate the water vapor budget and examine the relationship between the evolution of the precipitation and environmental forcing for Hurricanes Isidore and Lili (2002). The water budget parameters evaluated are the moisture flux convergence, ocean surface moisture flux, local change of TPW, cloud storage, and precipitation. Other environmental parameters examined include the mean SSTs, vertical wind shear, near-surface  $\theta_e$ , upper-tropospheric

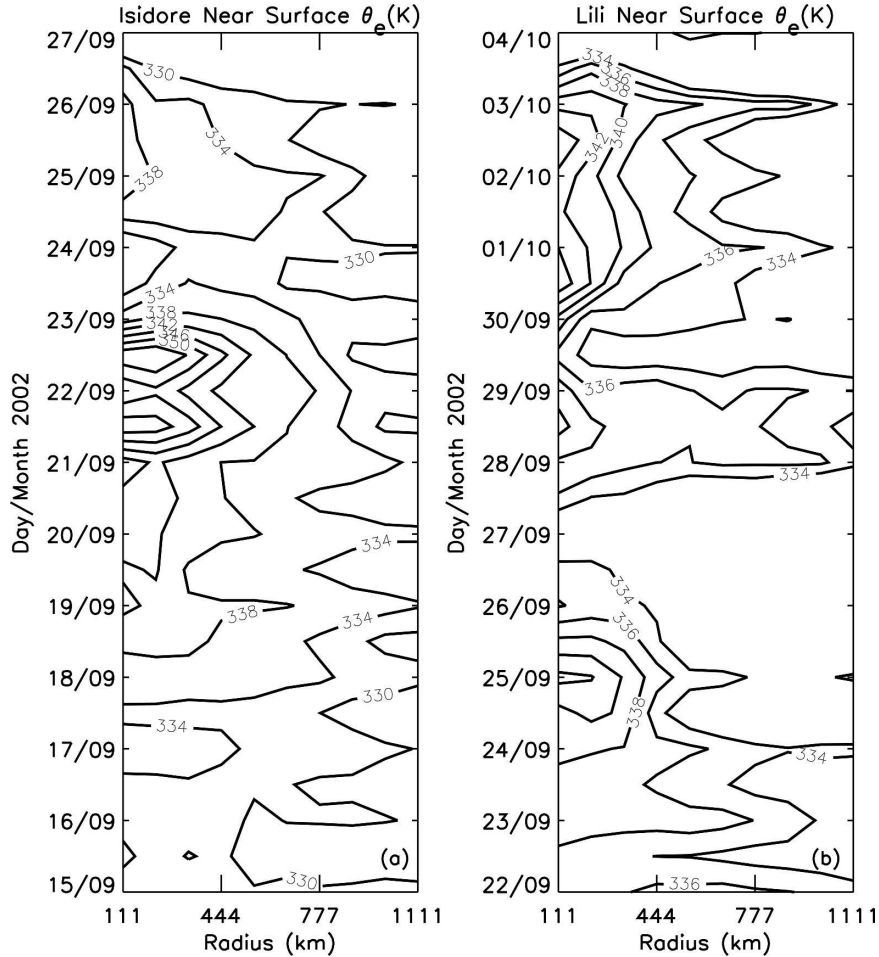


FIG. 12. Time–radius view of (a) Isidore’s and (b) Lili’s azimuthally averaged near-surface  $\theta_e$  derived from NOGAPS analyses for annuli 111 km in width extending 1111 km outward from the center.

divergence, TPW, near-surface sea surface – air moisture difference, and near-surface 10-m wind speed.

To first order, the larger diameter of Isidore is responsible for the greater rain volume in a Lagrangian framework, but it is not the only controlling factor. The evaluation of the water vapor budget presented in section 4 gives some insight into the important mechanisms that influence the precipitation distribution and storm wetness of Isidore and Lili. During the life cycle of these two storms, the moisture convergence appeared to be the dominant mechanism in producing the observed rainfall and cloud storage. Evaporation from the ocean surface was the second dominant term. The local change of the TPW term was relatively small, while the cloud storage term increased when the storm experienced an expansion in size and large moisture convergence and ocean evaporation. The cloud storage became negative during landfall through evaporation from rain and cloud.

The water budget confirms that the ocean moisture flux in the whole tropical cyclone region is substantial relative to the condensation and total moisture convergence, with the ocean moisture flux in the whole storm being approximately 47%–52% of the total condensation for large-sized storms (i.e., Isidore and Lili). This result is in agreement with Kurihara (1975) and Braun (2006), and suggests that the ocean source plays an important role in supplying moisture for precipitation processes when considering both inner and outer regions of the storm.

The magnitude and distribution of TPW appeared to be crucial to determining the total moisture convergence and, therefore, the storm total rain amount. During Isidore and Lili’s lifetime, Isidore’s volumetric TPW was larger and extended to larger radius than Lili’s. Figures 2–3 and 6–7 indicate higher TPW covering a broad area for Isidore compared with Lili. The reason that Isidore was so much wetter than Lili was that the



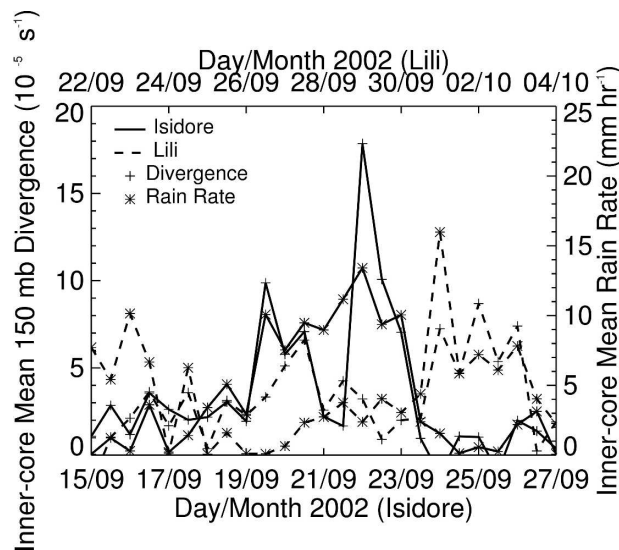


FIG. 13. The time change of the inner-core mean 150-mb divergence ( $10^{-5} \text{ s}^{-1}$ ) and the MPA-RT-derived inner-core mean rain rate ( $\text{mm h}^{-1}$ ) for Isidore and Lili.

far-field humidity environment was much moister for Isidore. Meanwhile, the period when Isidore reached its maximum wind intensity was coincident with the storm's interaction with the Yucatan. Both the frictional convergence and strong storm intensity play a role in the large moisture convergence of Isidore. Of course, the entire mixed ocean layer depth and temperature have been shown to be important; perhaps this effect can be investigated with more ocean data.

Mature tropical cyclones located over ocean regions with SST  $\leq 26^\circ\text{C}$  and weak vertical wind shear (e.g.,  $\leq 5 \text{ m s}^{-1}$ ) have the maximum potential to intensify and develop strong rain episodes. However, the impact of shear on total rain volume may be indirect through the impact of shear on storm intensity. Isidore's strongest rain episode during 22–25 September was related to weak vertical shear ( $\sim 4\text{--}5 \text{ m s}^{-1}$ ) and warm SSTs (nearly  $29.5^\circ\text{C}$ ). Lili encountered very low shear ( $0.2 \text{ m s}^{-1}$ ) and warm SST ( $28.9^\circ\text{C}$ ) on 28 September when Lili's volumetric rain reached a peak value.

High near-surface  $\theta_e$  around inner-core regions is found to be associated with the storm intensity. A similar relationship is found between the inner-core mean 150-mb divergence and storm inner-core mean rain rate. These relationships are consistent with other studies showing that high near-surface heat and moisture energy and upper-level outflow are probably necessary for storm intensification or rain potential.

The future work will focus on applying the current analysis method to a large sample of landfalling storms to understand the differences in tropical cyclone rain-

fall by relating it to the environmental parameters. Statistical relationships between storm volumetric rain and environmental parameters such as TPW, moisture convergence, and ocean moisture flux could be examined to see how well (or poorly) models can predict tropical cyclone rainfall.

*Acknowledgments.* The authors thank Drs. James Goerss and Liz Ritchie for providing very useful assistance concerning NOGAPS analyses. Thanks to Drs. Robert Adler and George Huffman for providing the MPA-RT data. The authors wish to acknowledge help from Mr. Hal Pierce for processing the MPA-RT data. Drs. Jan Paegle and Dean Duffy provided assistance with performing the water budget calculations. Thanks to Dr. Chuntao Liu for his help with obtaining the SSM/I data. Thanks are given to Manuel Lonfat for discussions and feedback. The constructive suggestions from three anonymous reviewers resulted in substantial improvements to the manuscript. This research was supported by a NASA TRMM grant. The authors thank Ramesh Kakar (NASA headquarters) for his continued support of TRMM science.

#### REFERENCES

- Awaka, J., T. Iguchi, and K. Okamoto, 1998: Early results on rain type classification by the Tropical Rainfall Measuring Mission (TRMM) Precipitation Radar. *Proc. Eighth URSI Commission F Open Symp.*, Aveiro, Portugal, Int. Union of Radio Science, 143–146.
- Bradbury, D. L., 1957: Moisture analysis and water budget in three different types of storms. *J. Meteor.*, **14**, 559–565.
- Braun, S. A., M. T. Montgomery, and Z. Pu, 2006: High-resolution simulation of Hurricane Bonnie (1998). Part I: The organization of eyewall vertical motion. *J. Atmos. Sci.*, **63**, 19–42.
- Carr, F. H., and L. F. Bosart, 1978: A diagnostic evaluation of rainfall predictability for Tropical Storm Agnes, June 1972. *Mon. Wea. Rev.*, **106**, 363–374.
- Challa, M., and R. Pfeffer, 1980: Effects of eddy flux of angular momentum on model hurricane development. *J. Atmos. Sci.*, **37**, 1603–1618.
- Charney, J. G., and A. Eliassen, 1964: On the growth of the hurricane depression. *J. Atmos. Sci.*, **21**, 68–75.
- DeMaria, M., J.-J. Baik, and J. Kaplan, 1993: Upper-level eddy angular momentum fluxes and tropical cyclone intensity change. *J. Atmos. Sci.*, **50**, 1133–1147.
- Emanuel, K. A., 1986: An air–sea interaction theory for tropical cyclones. Part I: Steady-state maintenance. *J. Atmos. Sci.*, **43**, 585–604.
- Frank, W. M., 1977: The structure and energetics of the tropical cyclone. Part I: Storm structure. *Mon. Wea. Rev.*, **105**, 1119–1135.
- , and E. Ritchie, 2001: Effects of vertical wind shear on the intensity and structure of numerically simulated hurricanes. *Mon. Wea. Rev.*, **129**, 2249–2269.
- Gamache, J. F., R. A. Houze, and F. D. Marks Jr., 1993: Dual-

- aircraft investigation of the inner core of Hurricane Norbert. Part III: Water budget. *J. Atmos. Sci.*, **50**, 3221–3243.
- Goerss, J. S., and P. A. Phoebus, 1992: The Navy's operational atmospheric analysis. *Wea. Forecasting*, **7**, 232–249.
- , and R. A. Jeffries, 1994: Assimilation of synthetic tropical cyclone observations into the Navy Operational Global Atmospheric Prediction System. *Wea. Forecasting*, **9**, 557–576.
- Gray, W. M., 1979: Hurricanes: Their formation, structure, and likely role in the tropical circulation. *Meteorology over the Tropical Oceans*, D. B. Shaw, Ed., Roy. Meteor. Soc., 155–218.
- Halverson, J., M. Garstang, J. Scala, and W.-K. Tao, 1996: Water and energy budgets of a Florida mesoscale convective system: A combined observational and modeling study. *Mon. Wea. Rev.*, **124**, 1161–1180.
- , J. Simpson, G. Heymsfield, H. Pierce, T. Hock, and L. Ritchie, 2006: Warm core structure of Hurricane Erin diagnosed from high-altitude dropsondes during CAMEX-4. *J. Atmos. Sci.*, **63**, 309–324.
- Hawkins, H. F., and D. T. Rubsam, 1968: Hurricane Hilda, 1964. II. Structure and budgets of the hurricane on October 1, 1964. *Mon. Wea. Rev.*, **96**, 617–636.
- , and S. M. Imbembo, 1976: The structure of a small, intense hurricane—Inez 1966. *Mon. Wea. Rev.*, **104**, 418–442.
- Heymsfield, G. M., J. B. Halverson, E. Ritchie, J. Simpson, J. Molinari, and L. Tian, 2005: Structure of the highly sheared Tropical Storm Chantal during CAMEX-4. *J. Atmos. Sci.*, **63**, 268–287.
- Hollinger, J. O., 1991: DMSR Special Sensor Microwave/Imager calibration/validation. Final Rep. Vol. 11, 1225 pp. [Available from J. O. Hollinger, Naval Research Laboratory, Washington, DC 20375.]
- Huffman, G. J., R. F. Adler, E. F. Stocker, D. T. Bolvin, and E. J. Nelkin, 2003: Analysis of TRMM 3-hourly multi-satellite precipitation estimates computed in both real and post-real time. Preprints, *12th Conf. on Satellite Meteorology and Oceanography*, Long Beach, CA, Amer. Meteor. Soc., P4.11.
- , and Coauthors, 2007: The TRMM Multisatellite Precipitation Analysis (TMPA): Quasi-global, multiyear, combined-sensor precipitation estimates at fine scales. *J. Hydrometeorol.*, **8**, 38–55.
- Jiang, H., 2004: Quantitative precipitation and hydrometeor content estimation in tropical cyclones from remote sensing observations. Ph.D. dissertation, University of Utah, Salt Lake City, UT, 207 pp.
- , and E. J. Zipser, 2006: Retrieval of hydrometeor profiles in tropical cyclones and convection from combined radar and radiometer observations. *J. Appl. Meteor.*, **45**, 1096–1115.
- , J. B. Halverson, and J. Simpson, 2008: On the differences in storm rainfall of Hurricanes Isidore and Lili. Part I: Satellite observations and rain potential. *Wea. Forecasting*, **23**, 29–43.
- Kummerow, C., W. S. Olson, and L. Giglio, 1996: A simplified scheme for obtaining precipitation and vertical hydrometeor profiles from passive microwave sensors. *IEEE Trans. Geosci. Remote Sens.*, **34**, 1213–1232.
- , and Coauthors, 2000: The status of the Tropical Rainfall Measuring Mission (TRMM) after two years in orbit. *J. Appl. Meteor.*, **39**, 1965–1982.
- Kurihara, Y., 1975: Budget analysis of a tropical cyclone simulated in an axisymmetric numerical model. *J. Atmos. Sci.*, **32**, 25–59.
- Liu, W. T., 1988: Moisture and latent heat flux variabilities in the tropical Pacific derived from satellite data. *J. Geophys. Res.*, **93**, 6749–6760.
- Lonfat, M., F. D. Marks, and S. S. Chen, 2004: Precipitation distribution in tropical cyclones using the Tropical Rainfall Measuring Mission (TRMM) Microwave Imager: A global perspective. *Mon. Wea. Rev.*, **132**, 1645–1660.
- Louis, J. F., 1979: A parametric model of vertical eddy fluxes in the atmosphere. *Bound.-Layer Meteorol.*, **17**, 187–202.
- Malkus, J., and H. Riehl, 1960: On the dynamics and energy transformations in steady-state hurricanes. *Tellus*, **12**, 1–20.
- Merrill, R. T., 1988: Environmental influence on hurricane intensification. *J. Atmos. Sci.*, **45**, 1678–1687.
- Molinari, J., and S. Skubis, 1985: Evolution of the surface wind field in an intensifying tropical cyclone. *J. Atmos. Sci.*, **42**, 2865–2879.
- , D. Vollaro, and K. L. Corbosiero, 2004: Tropical storm formation in a sheared environment: A case study. *J. Atmos. Sci.*, **61**, 2493–2509.
- Mundell, D. B., 1991: Tropical cyclone intensification. Preprints, *19th Conf. on Hurricanes and Tropical Meteorology*, Miami, FL, Amer. Meteor. Soc., 511–515.
- Rabin, R. M., L. A. McMurdie, C. M. Hayden, and G. S. Wade, 1993: Evaluation of the atmospheric water budget following an intense cold-air outbreak over the Gulf of Mexico—Application of a regional forecast model and SSM/I observations. *J. Appl. Meteor.*, **32**, 3–16.
- Rodgers, E. B., and H. F. Pierce, 1995: Environmental influence on Typhoon Bobbie's precipitation distribution. *J. Appl. Meteor.*, **34**, 2515–2532.
- , S. W. Chang, J. Stout, J. Steranka, and J.-J. Shi, 1991: Satellite observations of variations in tropical cyclone convection caused by upper-tropospheric troughs. *J. Appl. Meteor.*, **30**, 1163–1184.
- , J.-J. Baik, and H. F. Pierce, 1994: The environmental influence on tropical cyclone precipitation. *J. Appl. Meteor.*, **33**, 573–593.
- , W. S. Olson, V. M. Karyampudi, and H. F. Pierce, 1998: Satellite-derived latent heating distribution and environmental influences in Hurricane Opal (1995). *Mon. Wea. Rev.*, **126**, 1229–1247.
- , —, J. Halverson, J. Simpson, and H. F. Pierce, 2000: Environmental forcing of Supertyphoon Paka's (1997) latent heat structure. *J. Appl. Meteor.*, **39**, 1983–2006.
- Rosmond, T. E., 1992: The design and testing of the Navy Operational Global Atmospheric Prediction System. *Wea. Forecasting*, **7**, 262–272.
- Simpson, J., R. F. Adler, and G. R. North, 1988: A proposed Tropical Rainfall Measuring Mission (TRMM) satellite. *Bull. Amer. Meteor. Soc.*, **69**, 278–295.
- , C. Kummerow, W.-K. Tao, and R. F. Adler, 1996: On the Tropical Rainfall Measuring Mission (TRMM). *Meteor. Atmos. Phys.*, **60**, 19–36.
- Spar, J., 1953: A suggested technique for quantitative precipitation forecasting. *Mov. Wea. Rev.*, **81**, 217–221.
- Spencer, R. W., H. M. Goodman, and R. E. Hood, 1989: Precipitation retrieval over land and ocean with the SSM/I: Identification and characteristics of the scattering signal. *J. Atmos. Oceanic Technol.*, **6**, 254–273.
- Wentz, F. J., 1997: A well-calibrated ocean algorithm for Special Sensor Microwave/Imager. *J. Geophys. Res.*, **102**, 8703–8718.
- Zehr, R. M., 2003: Environmental vertical wind with Hurricane Bertha (1996). *Wea. Forecasting*, **18**, 345–356.